Numerical Modeling and Simulation of the Movable Contact Tool-Workpiece and Application in Technological Processes

Leon KUKIELKA, Agnieszka KULAKOWSKA, Radoslaw PATYK
Faculty of Mechanical Engineering, Koszalin University of Technology, Śniadeckich 2
Koszalin, 75-620, Poland

ABSTRACT

Grinding, embossing, burnishing, thread rolling, drawing, cutting, turning are very complicated technological processes. To increase the quality of the product and minimize the cost of process, we should know the physical phenomena which exist during the process. The phenomena on a typical incremental step were described using a step-by-step incremental procedure, with an updated Lagrange's formulation. The technological processes are considered as geometrical and physical non-linear initial and boundary problems. The finite element method (FEM) and the dynamic explicit method (DEM) were used to obtain the solution. The application was developed in the ANSYS/LS-DYNA system, which makes possible a complex time analysis of the physical phenomena: states of displacements, strains and stresses. Numerical computations of the strain and stress have been conducted with the use of methodology which requires a proper definition of the contact zone, without the necessity to introduce boundary conditions. Examples of calculations are presented.

Keywords: Technological Processes, Updated Lagrangian Formulation, FEM, DEM, Numerical Modeling, Numerical Simulation, Geometrical Contact Conditions.

1. INTRODUCTION

The technological processes as grinding, embossing, burnishing, thread rolling, drawing, cutting are very complicated. To increase the quality of the product and minimize the cost of process, we should know the physical phenomena which exist during the process. This paper presents the modeling and simulation of a contact problem in the operation of technological production of objects. The processes are considered as a geometrical and physical non-linear initial and boundary value problems. The mathematical model on a typical incremental step time were described using step-by-step procedure, with updated J.L. Lagrange's formulation [1]. A new incremental material model of elastic (domain reversible) and visco-plastic (domain non-reversible) with mixed hardening, including high strain rates and geometrical and physical nonlinearities is used. The model takes into account the history of deformation. The identification of constitutive parameters in the model of yield stress is made using unidirectional test on the studied different materials. An incremental model of the contact problem for movable elasto/visco-plastic body for spatial states (3D) is being considered. Geometrical contact conditions (GCC) for the case of a deformed object and a rigid or elastic tool, with a rotation and translation of the bodies are introduced. A GCC form used in numeric calculations is determined. Dependences between increments of unit forces in the contact area of bodies is introduced. Basic incremental equations of the edge displacement in the reversible and non reversible zone are defined. The description of a geometrical contact conditions and friction conditions in the ranges of stick-slip are considered. The models obtained are used to a variational formulation of equation of motion and deformation in three dimensions for this case. Then, the finite element method (FEM) and dynamic explicit method (DEM) were used to obtain the solution. The procedure has been implemented in the finite element computer program ANSYS, which makes possible a complex time analysis of the physical phenomena: states of displacements, strains and stresses. Numerical computations of the strain have been conducted with the use of methodology – a proper definition of the contact zone, without the necessity to introduce boundary conditions. Examples of numerical analysis of contact bodies (tool-object) in different technological operations as grinding and thread rolling processes are shown. The influence of the a single abrasive grain geometry and the cutting angle on the states of strain and stress in the surface layer during machining is explained. Examples of simulation of the influence a various thread rolling process conditions on the states of strain and stress, were presented.

2. MATHEMATICAL MODEL OF PROCESS

A mathematical model of the technological processes is formulated in increments and contains the following: a material model, a contact model, an equation of motion and deformation, with initial and boundary conditions.

Material model

Yield stress: Yield stress σ_y is the most important parameter characterizing the resistance of a visco-plastic deformation. The incremental model of the yield stress for a typical step time $t \to \tau = t + \Delta t$ was defined as [2]:

$$\Delta\sigma_Y = F_1(\cdot)\cdot\Delta\varepsilon_e^{(VP)} + F_2(\cdot)\cdot\Delta\dot{\varepsilon}_e^{(VP)}\ , \qquad (1)$$

where $\Delta\varepsilon_e^{(VP)}$ and $\Delta\dot{\varepsilon}_e^{(VP)}$ are the increment of effective visco-plastic strain and strain rate, respectively, $F_1(\cdot)\cdot\Delta\varepsilon_e^{(VP)}$ is the component of change in the temporary yield stress σ_Y with change of the visco-plastic strain, where $F_1(\cdot) = \partial\sigma_Y(\cdot)/\partial\varepsilon_e^{(VP)}$ is temporary hardening parameter for constant accumulated effective visco-plastic strain rate at time t $(\dot{\varepsilon}_e^{(VP)} = \text{const})$, $F_2(\cdot)\cdot\Delta\dot{\varepsilon}_e^{(VP)}$ is the component of change in the temporary yield stress σ_Y with change of the visco-plastic strain rate, where $F_2(\cdot) = \partial\sigma_Y(\cdot)/\partial\dot{\varepsilon}_e^{(VP)}$ is temporary hardening parameter for constant accumulated effective visco-plastic strain at time t $(\varepsilon_e^{(VP)} = \text{const})$.

Elastic/visco-plastic material model: A new model of mixed hardening for isotropic material which includes the combined effects of elasticity (reversible domain), visco-plasticity (non-reversible domain) (E/VP) is used. The model takes into account the history of the material.
The constitutive equation of increment components of a total strain tensor takes form:

$$\Delta\varepsilon_{ij} = \frac{1}{1-\tilde{S}^{**}}\cdot(D_{ijkl}^{(E)}\cdot\Delta\sigma_{kl} - A\cdot\tilde{S}_{ij}^{*}), \qquad (2)$$

and of increment components of the total stress tensor:

$$\Delta\sigma_{ij} = C_{ijkl}^{(E)}\cdot\Delta\varepsilon_{kl} - \psi\cdot\tilde{S}_{ij}^{*}\cdot(\tilde{S}_{ij}\cdot C_{ijkl}^{(E)}\cdot\Delta\varepsilon_{kl} - A), \qquad (3)$$

where:

$$\tilde{S}^{**} = \tilde{S}^{*}_{ij} \cdot C^{(E)}_{ijmn} \cdot \tilde{S}_{mn}, \tag{4}$$

is a positive scalar variable,

$$\tilde{S}^{*}_{ij} = \frac{\tilde{S}_{ij}}{\tilde{S}_{ij} \cdot C^{(E)}_{ijkl} \cdot \tilde{S}_{ij} + \frac{2}{3} \cdot \sigma_Y^2 \cdot (\tilde{C} + E_T)}, \tag{5}$$

is a component of a stress tensor,

$$A = \frac{2}{3} \cdot \sigma_Y \cdot \frac{\partial \sigma_Y}{\partial \dot{\varepsilon}_e^{(VP)}} \cdot \Delta \dot{\varepsilon}_e^{(VP)} \tag{6}$$

is a positive scalar variable, $\Delta\sigma_{ij}$ is the increment component of the second Piola-Kirchhoff stress tensor, $D^{(E)}_{ijkl}$ are the components of tensor $\mathbf{D}^{(E)} = [\mathbf{C}^{(E)}]^{-1}$ in time t, $\Delta\varepsilon_{ij}$ is the increment component of Green-Lagrange strain tensor, $C^{(E)}_{ijkl}$ are the components of elastic constitutive tensor $\mathbf{C}^{(E)}$.

Model of contact tool-object

The qualification of the area real shape of the bodies' contact zones is combined with the determination in these areas of the states of loading mechanics (pressures and forces of friction) and the state of the deformation of the object material, and the opposite. In practical considerations, these states are uncoupled in the way that the first one determines the shape and the field of the contact point area of bodies and then loads the result for these conditions. The above case of the contact problem has an essential meaning: the contact forces, contact stiffness, shape and field of the contact area of bodies, contact boundary conditions and friction conditions in this area.

Forces in the contact zones: In the time increment Δt increment of unit force $\Delta\mathbf{p}_N$ acted in a perpendicular direction to the contact surface, however increments of unit forces increments of unit forces $\Delta\mathbf{p}_{Tj}$ and $\Delta\mathbf{t}_{Tj}$, j=1,2 are tangential to this surface.

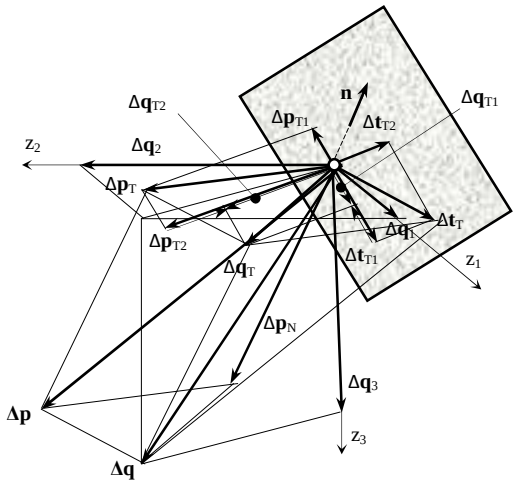

Figure1: Increments of unit forces in any point of contact zone

From Fig. 1, the following dependences result among increments of unit forces:

$$\Delta\mathbf{t}_T = \Delta\mathbf{t}_{T1} + \Delta\mathbf{t}_{T2},$$
$$\Delta\mathbf{p}_T = \Delta\mathbf{p}_{T1} + \Delta\mathbf{p}_{T2},$$
$$\Delta\mathbf{p} = \Delta\mathbf{p}_N + \Delta\mathbf{p}_T,$$
$$\Delta\mathbf{q}_T = \Delta\mathbf{q}_{T1} + \Delta\mathbf{q}_{T2} = \Delta\mathbf{t}_T + \Delta\mathbf{p}_T,$$
$$\Delta\mathbf{q} = \Delta\mathbf{q}_T + \Delta\mathbf{p}_N = \Delta\mathbf{p} + \Delta\mathbf{t}_T, \tag{7}$$

where $\Delta\mathbf{q}$ is the increment of the resultant unit force with components Δq_i, $i = 1 \div 3$.

The components of increment forces Δp_{Tj} and Δt_{Tj} add up yielding components Δq_{Tj} of resulting force $\Delta\mathbf{q}_T$, acting tangential to the surface of contact:

$$\Delta q_{Tj} = \Delta p_{Tj} \pm \Delta t_{Tj}, \ j = 1,2. \tag{8}$$

Contact stiffness: Contact forces cause the displacement of the edge of bodies in contact. The value of this displacement is dependent of the contact stiffness, which is defined by the relation of acting force onto the surface to the value of the displacement surface of the contact in the direction of the force working.

Contact stiffness occurs in the normal and tangential directions. Dependence of unit force-displacement ($p_i - u_i$) can be introduced with the help of two lines (Fig. 2). The first one concerns the range of the linear reversible displacement to yield stress p_i^y (range E), however the second one – the non-linear non-reversible displacement (range VP).

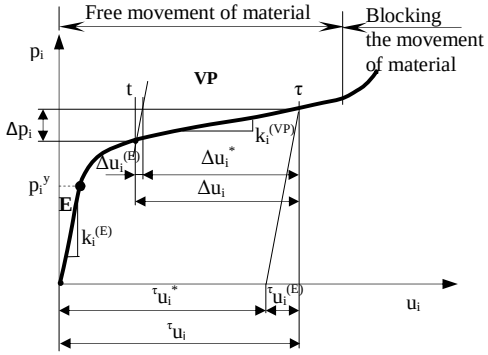

Figure 2: $p_i - u_i$ diagram for contact tool-object

An increment of the resulting displacement in the direction i, at a typical time increment, is calculated with the use of the following equation:

$$\Delta u_i = \Delta u_i^{(E)} + \Delta u_i^{*} \tag{9}$$

where $\Delta u_i^{(E)}$ is the increment of an elastic displacement, Δu_i^{*} is the increment of a visco-plastic displacement.
From $p_i - u_i$ diagram, we obtain:

$$\Delta p_i = k_i^{(E)} \cdot \Delta u_i^{(E)},$$
$$\Delta p_i = k_i^{(VP)} \cdot \Delta u_i, \tag{10}$$

where $k_i^{(E)}$ and $k_i^{(VP)}$ are temporary stiffness coefficients in direction i, for range E and VP respectively. This coefficients are given by:

$$k_i^{(E)} = \frac{\partial p_i}{\partial u_i}, \text{ for } p_i \le p_i^y,$$
$$k_i^{(E)} = \frac{p_i}{u_i^{(E)}}, \text{ for } p_i > p_i^y,$$
$$k_i^{(VP)} = 0, \text{ for } p_i \le p_i^y,$$
$$k_i^{(VP)} = \frac{\partial p_i}{\partial u_i}, \text{ for } p_i > p_i^y, \tag{11}$$

where $u_i^{(E)}$ is the accumulated component of elastic displacement, p_i is the accumulated component of the normal unit force at time t.

From Eqs. (10) and (11) we obtain the relations between the increment of resulting displacement Δu_i and the increment of pressure Δp_i:

$$\Delta u_i = [k_i^{(E)}]^{-1} \cdot \Delta p_i, \quad \text{for} \quad p_i \le p_i^y,$$
$$\Delta u_i = \Delta u_i^{(E)} + \frac{k_i^{(E)} - k_i^{(VP)}}{k_i^{(VP)} \cdot k_i^{(E)}} \cdot \Delta p_i, \quad \text{for} \quad p_i > p_i^y. \qquad (12)$$

It results from relationships Eq. (12) that the increment of the resulting unit force is the function of the increment of the edge displacement. The qualification of these relationships demands the knowledge of experimental curve $p_i - u_i$, for real conditions of the contact. It is often very difficult to realize the determination of such dependence, or it is unfeasible. In the present paper, this difficulty is eliminated by a variational formulation of movement equations and the use of iterative methods of solution. Assuming that the state of the increment of the pressure and frictions' force is known from the previous iteration, temporary coefficients of contact stiffness $k_i^{(E)}$ and $k_i^{(VP)}$ and dependence $p_i - u_i$ are determined analytically.

Boundary conditions in the contact zone: The geometrical condition of the contact defines current distance g between points on the edge of bodies along the normal direction, i.e. perpendicular to the tangential plane to both bodies (Fig. 3). A geometrical condition of the contact will become formulated in increments in a general form, i.e. for spatial states, at foundation, that both objects, as the tools undergo translation and turn, at which tool have much larger stiffness in comparison with the object. The bodies remain under influence of forces and moments.

Temporary distance ${}^{\tau}g(\mathbf{z},t)$ the edge of the object from the active surface of the tool, in a normal direction, following the dependence between the component vectors:

$${}^{\tau}g(z;\tau) = {}^{t}g(z;t) + \Delta K^{(t,o)} - \Delta u_3^{(o)}(z;\Delta t) - \Delta u_3^{(t)}(z;\Delta t) \ge 0, \quad (13)$$

where $\Delta K^{(t,o)}$ is a total influence of the translation increment and rotations of tools and the object onto the displacement increment of the object's edge $\Delta u_3^{(o)}(z;\Delta t)$ and tool $\Delta u_3^{(t)}(z;\Delta t)$.

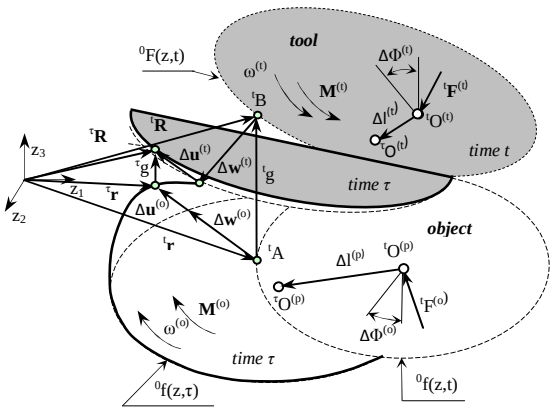

Figure 3: Illustration of geometrical conditions of contact

From condition Eq. (13), there result the following cases:

a) if ${}^{\tau}g(\cdot) > 0$ and ${}^{t}g(\cdot) > 0$ then the point in question lies beyond area of contact,
b) if ${}^{\tau}g(\cdot) = 0$ and ${}^{t}g(\cdot) > 0$ then in the considered point a contact followed,
c) if ${}^{\tau}g(\cdot) = 0$ and ${}^{t}g(\cdot) = 0$ then considered point in area of contact still stays in it,
d) if ${}^{\tau}g(\cdot) > 0$ and ${}^{t}g(\cdot) = 0$ then in the considered point a loss of contact occurred.

Condition Eq. (13) is used in numerical calculations. The application of an iterative procedure defines the displacement conditions in the contact area. Then, it takes root in the iteration process, that distance ${}^{\tau}g(\cdot) = 0$ and ${}^{t}g(\cdot) = 0$ (functions are known from foundation), increment of displacement of tool edge $\Delta u_3^{(o)}$ as a result of deformation is known from previous iteration, however it seeks itself an increment of the edge displacement of object $\Delta u_3^{(t)}$, from transformed Eq. (13) to form:

$$\Delta u_3^{(o)}(z;\Delta t)^{[i]} = \Delta K^{(t,o)}(\cdot)^{[i]} - \Delta u_3^{(t)}(z;\Delta t)^{[i-1]}. \qquad (14)$$

Boundary conditions for displacement Eq. (14) are applied in numerical analysis of the contact problem in consideration.

Incremental model of motion and deformation

Variational formulation: The equation of motion and deformation of the object is developed in the updated Lagrange's formulation. Assuming that numerical solutions are obtained at discrete time t, the solution for time $t + \Delta t$ is to be obtained. At this case a functional increment is formulated for increment displacement $\Delta\mathbf{F}[\Delta\ddot{u}_i, \Delta\dot{u}_i, \Delta u_i] = \Delta\mathbf{F}(\cdot)$, where Δu_i, $\Delta\dot{u}_i$, $\Delta\ddot{u}_i$ are the i*th* increment components of the displacement, velocity and acceleration vectors, respectively. Using the conditions of stationary of functional $\Delta\mathbf{F}(\cdot)$, we obtain a variational equation of motion and deformation:

$$\delta[\Delta\mathbf{F}(\cdot)] = \int_{{}^tV} \rho\cdot(\ddot{u}_i + \Delta\ddot{u}_i)\cdot\delta(\Delta u_i)\cdot dV + \alpha\cdot\int_{{}^tV}\rho\cdot\Delta\dot{u}_i\cdot\delta(\Delta u_i)\cdot dV$$
$$-2\omega\cdot\int_{{}^tV}\rho\cdot\Delta\dot{u}_i\cdot\Omega_{ij}\cdot\delta(\Delta u_j)\cdot dV + \frac{1}{2}\cdot\beta\cdot\int_{{}^tV}\Delta\dot{\tilde{\varepsilon}}_{ij}\cdot C_{ijkl}^{(E)}\cdot\delta(\Delta\tilde{\varepsilon}_{kl})\cdot dV$$
$$+\frac{1}{2}\cdot\beta\cdot\int_{{}^tV}\Delta\dot{\tilde{\varepsilon}}_{ij}\cdot C_{ijkl}^{(E)}\cdot\delta(\Delta\bar{\varepsilon}_{kl})\cdot dV + \frac{1}{2}\cdot\beta\cdot\int_{{}^tV}\Delta\dot{\bar{\varepsilon}}_{ij}\cdot C_{ijkl}^{(E)}\cdot\delta(\Delta\tilde{\varepsilon}_{kl})\cdot dV$$
$$+\frac{1}{2}\cdot\beta\cdot\int_{{}^tV}\Delta\dot{\bar{\varepsilon}}_{ij}\cdot C_{ijkl}^{(E)}\cdot\delta(\Delta\bar{\varepsilon}_{kl})\cdot dV + \frac{1}{2}\cdot\beta\cdot\int_{{}^tV}\delta(\Delta\dot{\tilde{\varepsilon}}_{kl})\cdot C_{ijkl}^{(E)}\cdot\Delta\tilde{\varepsilon}_{kl}\cdot dV$$
$$+\frac{1}{2}\cdot\beta\int_{{}^tV}\delta(\Delta\dot{\bar{\varepsilon}}_{kl})\cdot C_{ijkl}^{(E)}\cdot\Delta\bar{\varepsilon}_{kl}\cdot dV + \frac{1}{2}\cdot\beta\cdot\int_{{}^tV}\delta(\Delta\dot{\bar{\varepsilon}}_{kl})\cdot C_{ijkl}^{(E)}\cdot\Delta\tilde{\varepsilon}_{kl}\cdot dV$$
$$+\frac{1}{2}\cdot\beta\cdot\int_{{}^tV}\delta(\Delta\dot{\bar{\varepsilon}}_{kl})\cdot C_{ijkl}^{(E)}\cdot\delta(\Delta\bar{\varepsilon}_{kl})\cdot dV + \int_{{}^tV}\Delta\tilde{\varepsilon}_{ij}\cdot C_{ijkl}^{(E)*}\cdot\delta(\Delta\tilde{\varepsilon}_{kl})\cdot dV$$
$$+\int_{{}^tV}\Delta\tilde{\varepsilon}_{ij}\cdot C_{ijkl}^{(E)*}\cdot\delta(\Delta\bar{\varepsilon}_{kl})\cdot dV + \int_{{}^tV}\Delta\bar{\varepsilon}_{ij}\cdot C_{ijkl}^{(TE)*}\cdot\delta(\Delta\tilde{\varepsilon}_{kl})\cdot dV$$
$$+\int_{{}^tV}\Delta\bar{\varepsilon}_{ij}\cdot C_{ijkl}^{(TE)*}\cdot\delta(\Delta\bar{\varepsilon}_{kl})\cdot dV + \frac{1}{2}\cdot\int_{{}^tV}(T_{ij} + \Delta\sigma_{ij}^{**})\cdot\delta(\Delta\tilde{\varepsilon}_{kl})\cdot dV$$
$$+\frac{1}{2}\cdot\int_{{}^tV}(T_{ij} + \Delta\sigma_{ij}^{**})\cdot\delta(\Delta\bar{\varepsilon}_{kl})\cdot dV - \omega^2\cdot\int_{{}^tV}\rho\cdot r_i\cdot\Omega_{ij}\cdot\Omega_{ij}\cdot\delta(\Delta u_i)\cdot dV$$
$$-\int_{{}^tV}\rho\cdot(f_i + \Delta f_i)\cdot\delta(\Delta u_i)\cdot dV - \int_{{}^t\Sigma_k}(\hat{q}_i + \Delta\hat{q}_i)\cdot\delta(\Delta u_i)\cdot d\Sigma_k = 0, \quad (15)$$

where T_{ij} is the component of Cauchy's stress tensor, α and β are constants (to be determined from two given damping ratios that correspond to two unequal frequencies of vibration), $\Delta\dot{\bar{\varepsilon}}_{ij}$, $\Delta\dot{\tilde{\varepsilon}}_{ij}$ are linear and non-linear increment components of

Green-Lagrange's strain rate tensor, $\Delta\bar{\varepsilon}_{ij} = 0{,}5\cdot(\Delta u_{i,j} + \Delta u_{j,i})$ and $\Delta\tilde{\varepsilon}_{ij} = 0{,}5\cdot(\Delta u_{i,k}\cdot\Delta u_{j,k})$ are the linear and non-linear increments components of Green-Lagrange's strain tensor, respectively, ρ is the mass density at time t, ε_{ij} is a accumulated component of total strain tensor at time t (depend on the history of deformation), f_i, Δf_i are the components of the internal force and increment force vectors, respectively, q_i, Δq_i are the components of the externally applied surface force and surface increment force vectors in the contact body zones, respectively, Ω_{ij} is the component of the gyro tensor. The integrations are performed over the volume V and surface Σ of the body, respectively.

Implementation of the finite elements method: Assume that the complete body under consideration has been idealized as an assemblage of finite elements, we have, at typical step time $t \to \tau = t + \Delta t$ for element e, in the local coordinate $\{\mathbf{x}\}$:

$$\begin{aligned}
\Delta\mathbf{u}^{(e)} &= \mathbf{N}^{(e)}\cdot\Delta\mathbf{w}^{(e)},\\
\Delta\dot{\mathbf{u}}^{(e)} &= \mathbf{N}^{(e)}\cdot\Delta\dot{\mathbf{w}}^{(e)},\\
\Delta\ddot{\mathbf{u}}^{(e)} &= \mathbf{N}^{(e)}\cdot\Delta\ddot{\mathbf{w}}^{(e)}\\
\Delta\bar{\boldsymbol{\varepsilon}}^{(e)} &= \bar{\mathbf{B}}^{(e)}\cdot\Delta\mathbf{w}^{(e)},\\
\Delta\dot{\bar{\boldsymbol{\varepsilon}}}^{(e)} &= \bar{\mathbf{B}}^{(e)}\cdot\Delta\dot{\mathbf{w}}^{(e)} + \dot{\bar{\mathbf{B}}}^{(e)}\cdot\Delta\mathbf{w}^{(e)},\\
\Delta\tilde{\boldsymbol{\varepsilon}}^{(e)} &= \Delta\bar{\mathbf{w}}^{(e)}\cdot\tilde{\mathbf{B}}^{(e)}\cdot\Delta\mathbf{w}^{(e)},\\
\Delta\dot{\tilde{\boldsymbol{\varepsilon}}}^{(e)} &= 2\cdot\Delta\bar{\mathbf{w}}^{(e)}\cdot\tilde{\mathbf{B}}^{(e)}\cdot\Delta\dot{\mathbf{w}}^{(e)},\\
\Delta\boldsymbol{\sigma}^{(e)} &= (\mathbf{S}^{(e)} + \mathbf{C}^{(E)(e)}\cdot\Delta\bar{\mathbf{w}}^{(e)}\cdot\tilde{\mathbf{B}}^{(e)})\cdot\Delta\mathbf{w}^{(e)},
\end{aligned}\qquad (16)$$

where $\Delta\mathbf{w}^{(e)}, \Delta\dot{\mathbf{w}}^{(e)}, \Delta\ddot{\mathbf{w}}^{(e)}$ are increments vectors of displacement, velocity and acceleration in the all $W_{(e)}$ nodal points of element e, respectively, $\Delta\bar{\mathbf{w}}^{(e)}$ is the matrix of displacements increments, the $\mathbf{N}^{(e)}$ is displacement interpolation matrix, $\bar{\mathbf{B}}^{(e)}$, $\tilde{\mathbf{B}}^{(e)}$ are linear and non-linear incremental strain - incremental displacement transformation matrices, $\mathbf{S}^{(e)}$ now define the incremental stress within element e as a function of the nodal point incremental displacement.

The variations in the Eq. (15) in the local Cartesian coordinate $\{\mathbf{x}\}$ is:

$$\begin{aligned}
\delta(\Delta\mathbf{u}^{(e)}) &= \mathbf{N}^{(e)}\cdot\delta(\Delta\mathbf{w}^{(e)}),\\
\delta(\Delta\bar{\boldsymbol{\varepsilon}}^{(e)}) &= \bar{\mathbf{B}}^{(e)}\cdot\delta(\Delta\mathbf{w}^{(e)}),\\
\delta(\Delta\tilde{\boldsymbol{\varepsilon}}^{(e)}) &= \Delta\bar{\mathbf{w}}^{(e)}\cdot\tilde{\mathbf{B}}^{(e)}\cdot\delta(\Delta\mathbf{w}^{(e)})\\
\delta(\Delta\dot{\bar{\boldsymbol{\varepsilon}}}^{(e)}) &= \dot{\bar{\mathbf{B}}}^{(e)}\cdot\delta(\Delta\mathbf{w}^{(e)}),\\
\delta(\Delta\dot{\tilde{\boldsymbol{\varepsilon}}}^{(e)}) &= \Delta\dot{\bar{\mathbf{w}}}^{(e)}\cdot\tilde{\mathbf{B}}^{(e)}\cdot\delta(\Delta\mathbf{w}^{(e)}).
\end{aligned}\qquad (17)$$

Using the Eqs. (16) and (17) and substituting into the variational Eq. (15), we obtain the discretized equations of motion for an assemblage of elements in the global coordinate $\{\mathbf{z}\}$:

$$\begin{aligned}
&\mathbf{M}\Delta\ddot{\mathbf{r}} + \left\langle\mathbf{C}(\alpha,\beta,\mathbf{w},\Delta\mathbf{w},\Delta\mathbf{w}^2) + \mathbf{C}_G(\omega)\right\rangle\Delta\dot{\mathbf{r}} + \left\langle(1-S^{**})\left(\mathbf{K}_1^k + \mathbf{K}_1^u(\mathbf{w},\mathbf{w}^2)\right.\right.\\
&\left.\left. + \Delta\mathbf{K}_4(\mathbf{w},\Delta\mathbf{w}) + \Delta\mathbf{K}_5(\Delta\mathbf{w}^2)\right) + \mathbf{K}_2(\beta,\mathbf{w},\dot{\mathbf{w}}) - \mathbf{K}_C(\omega^2) + \mathbf{K}_1^\sigma(\sigma)\right.\\
&\left. + \Delta\mathbf{K}_1^\sigma(\Delta\sigma^{**}) + \Delta\mathbf{K}_3(\beta,\mathbf{w},\dot{\mathbf{w}},\Delta\mathbf{w},\Delta\dot{\mathbf{w}})\right\rangle\Delta\mathbf{r} = \mathbf{F}(\mathbf{f},\sigma,\ddot{\mathbf{w}}) + \mathbf{F}(\omega^2)\\
&+ \mathbf{R}(\hat{\mathbf{q}}) + \{\Delta\mathbf{F}(\Delta\mathbf{f},\Delta\sigma^{**}) + \Delta\mathbf{R}(\Delta\hat{\mathbf{q}}),
\end{aligned}\qquad (18)$$

where:

$$\begin{aligned}
\Delta\mathbf{w}^{(e)}{}_{W_{(e)}x1} &= \mathbf{A}^{(e)}{}_{W_{(e)}xN}\cdot\Delta\mathbf{r}_{Nx1},\\
\mathbf{A}^{(e)}{}_{W_{(e)}xN} &= \mathbf{A}_1^{(e)}{}_{W_{(e)}xW_{(e)}}\cdot\mathbf{A}_2^{(e)}{}_{W_{(e)}xN},
\end{aligned}\qquad (19)$$

$\mathbf{A}_1^{(e)}$ is the transformation matrix to relate the basis of local system $\{\mathbf{x}\}$ and global system $\{\mathbf{z}\}$, $\mathbf{A}_2^{(e)}$ is the Boole's matrix (logic matrix), $\Delta\mathbf{w}^{(e)}$ is the nodal point increment displacement vector of element e in the local coordinate $\{\mathbf{x}\}$, $\Delta\mathbf{r}$ is the nodal point increment displacement vector of system in the global coordinate $\{\mathbf{z}\}$, N is the number of all nodal points of system. Introduced the following notation:

$$\begin{aligned}
\mathbf{C}_T &= \mathbf{C}(\alpha,\beta,\mathbf{w},\Delta\mathbf{w},\Delta\mathbf{w}^2) + \mathbf{C}_G(\omega),\\
\mathbf{K}_T &= (1-{}_t^tS^{**})\left\langle\mathbf{K}_1^k + \mathbf{K}_1^u(\cdot)\right\rangle + \mathbf{K}_2(\cdot) - \mathbf{K}_C(\cdot) + \mathbf{K}_1^\sigma(\cdot),\\
\Delta\mathbf{K}_T &= (1-{}_t^tS^{**})\left\langle\Delta\mathbf{K}_4(\cdot) + \Delta\mathbf{K}_5(\cdot)\right\rangle + \Delta\mathbf{K}_1^\sigma(\cdot) + \Delta\mathbf{K}_3(\cdot),\\
\mathbf{F}_T &= \mathbf{F}(\mathbf{f},\sigma,\ddot{\mathbf{w}}) + \mathbf{F}(\omega^2) + \mathbf{R}(\hat{\mathbf{q}}),\\
\Delta\mathbf{F} &= \Delta\mathbf{F}(\Delta\mathbf{f},\Delta\sigma^{**}),\ \Delta\mathbf{R} = \Delta\mathbf{R}(\Delta\hat{\mathbf{q}}),
\end{aligned}\qquad (20)$$

we can write the Eq. (18) in the form:

$$\mathbf{M}\cdot\Delta\ddot{\mathbf{r}} + \mathbf{C}_T\cdot\Delta\dot{\mathbf{r}} + (\mathbf{K}_T + \Delta\mathbf{K}_T)\cdot\Delta\mathbf{r} = \Delta\mathbf{R} + \Delta\mathbf{F} + \mathbf{F}_T \quad (21)$$

where mass matrix $\mathbf{M}$, damping matrix $\mathbf{C}_T$, stiffness matrix $\mathbf{K}_T$ and external and internal force vector $\mathbf{F}_T$ are known at time t. However, increment stiffness matrix $\Delta\mathbf{K}_T$, external incremental load vector $\Delta\mathbf{R}$, internal incremental forces vector $\Delta\mathbf{F}$, incremental vectors of displacement $\Delta\mathbf{r}$, velocity $\Delta\dot{\mathbf{r}}$ and acceleration $\Delta\ddot{\mathbf{r}}$ of finite element assembly at a typical step time are not known. In order to solve this problem we apply the integration methods - central difference method (DEM), which it is one of methods of direct integration the Eq. (21).

3. DEM SOLUTION

Assuming that an increment of temporary step Δt is very small, it is possible to execute a linearization of Eq. (21) and using the incremental decomposition we obtain an equation for time t:

$$\mathbf{M}\cdot{}^t\ddot{\mathbf{r}} + \mathbf{C}_T\cdot{}^t\dot{\mathbf{r}} + \mathbf{K}_T\cdot{}^t\mathbf{r} = {}^t\mathbf{F}_T + {}^t\mathbf{Q}. \quad (22)$$

Then using the central difference method (DEM), in which it is assumed that:

$${}^t\dot{\mathbf{r}} = \frac{{}^{t+\Delta t}\mathbf{r} - {}^{t-\Delta t}\mathbf{r}}{2\cdot\Delta t},\quad {}^t\ddot{\mathbf{r}} = \frac{{}^{t+\Delta t}\mathbf{r} - 2\cdot{}^t\mathbf{r} + {}^{t-\Delta t}\mathbf{r}}{\Delta t^2} \quad (23)$$

and substituting the Eqs. (23) into Eq. (22) we obtain:

$$\tilde{\mathbf{M}}\cdot{}^\tau\mathbf{r} = {}^t\tilde{\mathbf{Q}}_T \quad (24)$$

where:

$$\tilde{\mathbf{M}} = \frac{\mathbf{M}}{\Delta t^2} + \frac{\mathbf{C}_T}{2\cdot\Delta t}$$

is effective mass matrix, and

$${}^t\tilde{\mathbf{Q}}_T = {}^t\mathbf{F}_T + {}^t\mathbf{Q} - \mathbf{K}_T\cdot{}^t\mathbf{r} + \frac{2\cdot{}^t\mathbf{r} - {}^{t-\Delta t}\mathbf{r}}{\Delta t^2}\cdot\mathbf{M} + \frac{{}^{t-\Delta t}\mathbf{r}}{2\cdot\Delta t}\cdot\mathbf{C}_T \quad (25)$$

is effective loads.

The integration method requires that the time step Δt is smaller than critical value Δt_{kr}, which can be calculated from the mass and stiffness properties of the complete element assemblage: $\Delta t \le \Delta t_{kr} = T_N/\pi$, where T_N is the smallest period of the finite element assemblage with N degrees of freedom.

4. RESULTS OF NUMERICAL CALCULATIONS

Rolling process of the round thread [3]

The main aim of the simulation was to define the influence of friction coefficient on the state of deformation (displacements and strain) and stress in the surface layer of the object. The numerical analysis for 2D states of deformation and 3D states of stress was applied on the example of steel C55. The tool is considered as rigid $E \to \infty$ or elastic body, however the material model as an elsto/visco-plastic body with non-linear hardening. The model has discretized by finite element PLANE183 with non-linear function of the shape. The contact tool with work pieces was modeling by elements TARGE169 and CONTA171.

Exemplary results of the numerical simulation are present on Figs 4 and 5. Analyzing the distribution of deformation of the finite element grid and state of effective strains and stresses, where the influence of the lubrication condition is observed.

For $\mu = 0$ in the contact zone tool – work piece (Fig. 4a), during the forming the outline of the thread, material isn't braking by tool and slide through the contact surface. The curving of vertical line of the finite element grid is invisible. Other side, increase the friction coefficient causes increase braking of the material. For high value of the friction coefficient (Fig. 4b) occurs strong braking of material in the contact zone. Form also the adhesion zone of material. That cause higher displacements of material in the zone placed father from the contact zone. Then the line of the finite element grid are stronger curved.

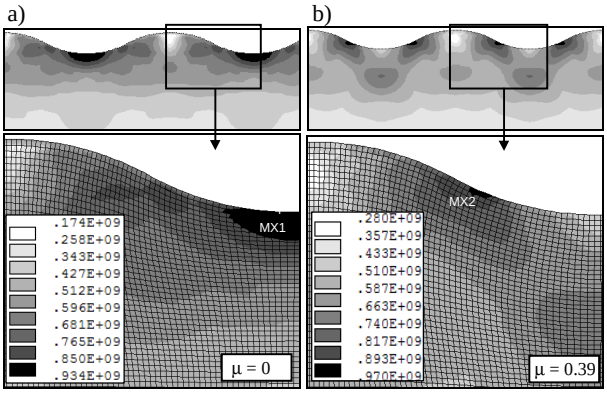

Figure 4: The deformation of grid and the maps of effective stresses on a longitudinal cutting plane for various value of frictions coefficient

The friction coefficient has high influence on value and distribution of strain. For $\mu = 0$ the maximum of effective strain $\varepsilon_e = 0{,}78$ is located on the bottom of the thread, near to the contact surface (MX1, Fig. 5a). For $\mu > 0$ appear an adhesion zone of material in the bottom of the thread, which take characteristic shape of a wedge. In this zone the value of strain is very small. For $\mu = 0{,}39$ strains are closer to the contact surface and getting smaller to value $\varepsilon_e = 0{,}0016$ (elastic strains) (MN, Fig. 5b). Whereat the local maximum of strains (MX1) moving down in surface layer. Then appear additional two local maximums of the effective strains. Second maximum (MX2) is placed near to the contact zone of the side of the thread, where higher value of friction coefficient increase strains value from $\varepsilon_e = 0{,}176$ for $\mu = 0$ (Fig.5a) to value $\varepsilon_e = 0{,}54$ for $\mu = 0{,}39$ (MX2, Fig.5b). Next one local maximum (MX3) is located in depth of material on symmetry axis pass through top of the thread. Here, strains are getting smaller together with increasing of friction coefficient from value $\varepsilon_e = 0{,}351$ for $\mu = 0$ (Fig. 5a) to $\varepsilon_e = 0{,}423$ for $\mu = 0{,}39$ (Fig. 5b).

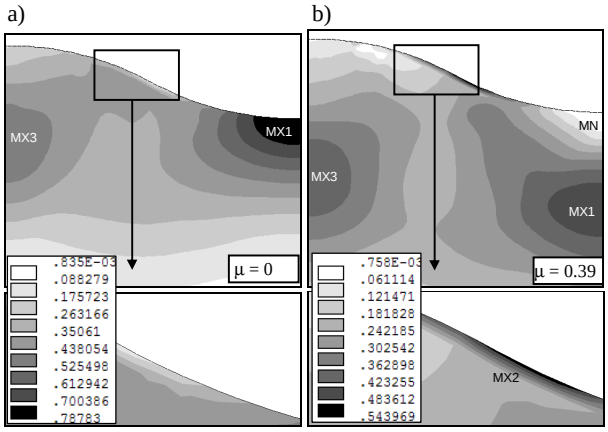

Figure 5: The maps of effective strains on a longitudinal cutting plane for various value of friction coefficient

Grinding process [5]

For the correct modelling and analysis of the grinding process, the knowledge of the course of the physical phenomena occurring in the machining zone in real conditions (i.e. geometry of grain and technological parameters) proves to be necessary. For this purpose, an analysis of the process of cutting with a single abrasive grain was conducted. The model of abrasive grain (Fig. 6) specified in paper [4] is considered as rigid or elastic body. The object is considered as the elastic/visco–plastic body and it's rotating with angular velocity ω around own axe. An abrasive grain with the apex angle of $\beta = 80 \div 120^o$ and the corner radius $r = 0{,}001$ μm is tilted in relation to the foundation by tool cutting edge angle $\alpha = \Phi + \theta + \gamma = 45 \div 65^o$ [6]. The depth of cut was $g = 0{,}01$ μm. The value of the real depth of cut of the material removed as a result of elastic displacement was smaller and was ca. $g_r = 0{,}009$ μm.

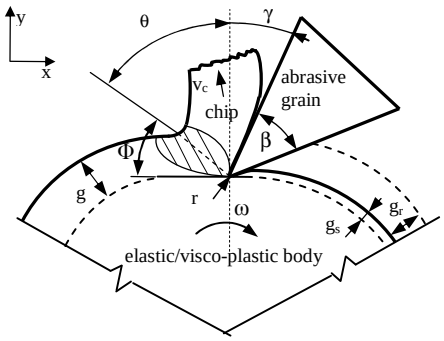

Figure 6: The schema of considered process of cutting with one abrasive grain the elastic/visco-plastic body: g – depth of cut, g_r – real depth of cut, g_s – elastic deformation of material, r – corner radius, v_c – chip velocity, ω – angular velocity, γ – tool rake angle, Φ – shear angle

Numerical simulation in the ANSYS system was conducted for different angles β and α of the abrasive grain. The object machined and the abrasive grain were digitized by elements of PLANE162 type with a non-linear function of shape. The contact grain with body was modeling by Single Surface Auto

2D (ASS2D). The net of finished elements was concentrated in the contact area. Sample simulation results are presented in Figs. 7 and 8.

While analysing the results obtained it was found that together with the change of the angles α and β, the values of strains and stresses are subject to change. Abrupt increases of stresses are the result of the chip creation phenomenon. Together with the increase of the tool cutting edge angle, the shear angle Φ of the material separated from the foundation increases, as well. It was found that both angles have a significant influence on the chip shape.

For the tool cutting edge angle $\alpha = 45^o$, we observe fast disturbances of the cohesion of the material between the neighbouring chip elements. This results in the fact that the chip drops off from the cutting edge in the form of separate elements – a segmental chip (Fig. 7).

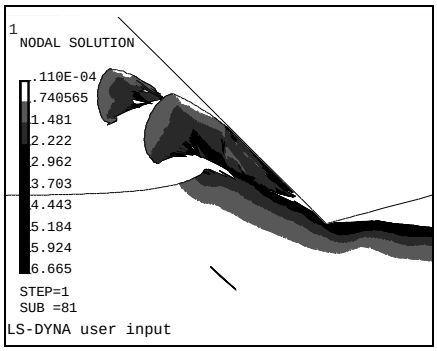

Figure 7: Map of effective strains in the chip creation phase for $\beta = 120^o$, $\alpha = 45^o$, r = 0,001 μm

For angle $\alpha = 65^o$, there occurs the phenomenon of chip curling (Fig. 8) in the direction of the foundation machined – a stepped chip. This is the result of the fact that the chip line from the side of the cutting edge action surface is longer than the chip line on its opposite side. For angle $\alpha = 55^o$, the chips created are segment chips. Fast cracking of the chip elements is observed.

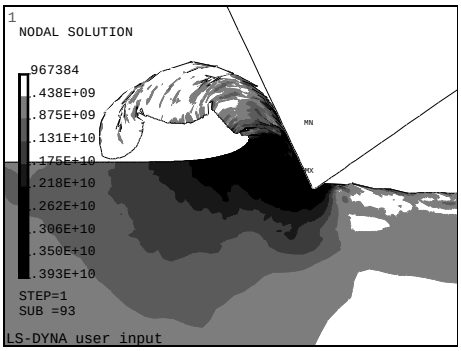

Figure 8: Map of effective stresses in the chip creation phase for $\beta = 80^o$, $\alpha = 65^o$, r = 0,001 μm

6. CONCLUSIONS

The technological processes are geometrical and physical non-linear initial and boundary problem. Boundary conditions in the contact zone tool-object are not determined. Measurement of a process parameters decide on the technological quality, such as: displacement, strain, stress, etc. during the process with nowadays technique of a measurement is impossible. About their course, we could conclude on the property of the product.

An application of modern mathematical modelling, numerical methods and computing systems allows an analysis of complex physical phenomena occurring in the process under investigation. The application developed in the ANSYS system enables a time analysis of the process with the consideration of the changeability of the lubrications conditions. On the course of physical phenomena in the working zone we can forecast a technological quality of the product.

The obtained results of the computer simulation of the thread rolling process show that the friction coefficient influence on the states of displacements, strains and stresses in the surface layer of the thread, also is one of the factors deciding about the technological and the exploitation quality. The best operational quality of the thread is received during the rolling process on great lubrication conditions ($\mu = 0$).

The simulation results for condition of lubrication can be use of while to designing the round thread rolling process: making a selection of the process condition and kind of the lubrication factor in the aspect of the technological quality of the thread.

The obtained results of the computer simulation of the cutting process with a single abrasive grain with a geometry of $2\theta = 120^o$ and cutting edge angle $\alpha = 45^o$ coincide with the results obtained by Kita and Ido [2]. The material flashes obtained before the grain cutting edge and its shapes similar to the results of experiential investigations confirm the justifiability of the use of computer simulations and their reliability.

The distributions of stresses and strains obtained for different grain geometries and action angles, on particular phases of the deformation process, can be made use of while designing machining: making a selection of the machining conditions and its optimising in the aspect of the technological quality of the product.

The distributions of stresses and strains obtained for different grain geometries and action angles, on particular phases of the deformation process, can be made use of while designing machining: making a selection of the machining conditions and its optimising in the aspect of the technological quality of the product.

7. REFERENCES

[1] K.J. Bathe, **Finite Element Procedures in Engineering Analisis**, Prentice – Hall, Englewood Cliffs, N.J., 1982.

[2] Y. Kita, M. Ido, "The mechanism of metal removal by abrasive tool", **Wear,** No. 1, 1978, pp. 185-193.

[3] K. Kukielka, L. Kukielka, "Modeling And Numerical Analysis Of The Thread Rolling Process", **WILEY-VCH Verlag GmbH & Co. KGaA**, Vol. 6, Issue 1, 2006, pp. 745-746.

[4] L. Kukielka, J. Kustra, "Numerical analysis of thermal phenomena and deformations in processing zone in the centreless continuous grinding process", **Computation Methods and Experimental Measurements for Surface Treatment Effects**, WIT*PRESS*, Southampton, Boston, 2003, pp.109-118.

[5] L. Kukiełka, J. Chodór, "Numerical analysis of chip formation during machining for different value of failure strain", **Journal PAMM**, Vol. 7, Issue 1, 2008, pp. 4030031-4030032.

[6] W. Lortz, "A model of the cutting mechanism in grinding", **Wear,** No. 53, 1979, pp. 115-128.